11-1-2023

Platinum single atoms anchored on ultra-thin carbon nitride nanosheets for photoreforming of glucose

Jinqiang Zhang

Xinyuan Xu
Edith Cowan University

Yazi Liu

Xiaoguang Duan

Shaobin Wang

See next page for additional authors

10.1016/j.surfin.2023.103423
Zhang, J., Xu, X., Liu, Y., Duan, X., Wang, S., & Sun, H. (2023). Platinum single atoms anchored on ultra-thin carbon nitride nanosheets for photoreforming of glucose. Surfaces and Interfaces, 42(Part A), article 103423. https://doi.org/10.1016/j.surfin.2023.103423

Surfaces and Interfaces 42 (2023) 103423

Contents lists available at ScienceDirect

Surfaces and Interfaces

journal homepage: www.sciencedirect.com/journal/surfaces-and-interfaces

Platinum single atoms anchored on ultra-thin carbon nitride nanosheets for photoreforming of glucose

Jinqiang Zhang [a,*], Xinyuan Xu [b,c], Yazi Liu [d], Xiaoguang Duan [a], Shaobin Wang [a], Hongqi Sun [b]

[a] School of Chemical Engineering, The University of Adelaide, SA 5005, Australia
[b] School of Molecular Sciences, The University of Western Australia, 35 Stirling Highway, Perth, WA 6009, Australia
[c] School of Science, Edith Cowan University, Joondalup, WA 6027, Australia
[d] School of Environment, Nanjing Normal University, Jiangsu Engineering Lab of Water and Soil Eco-Remediation, Nanjing 210023, PR China

ARTICLE INFO

Keywords:
Pt single atom
Carbon nitride
Pumping effect
Hydrogen production
Biomass photoreforming

ABSTRACT

Photoreforming of biomass is a fascinating process that harnesses renewable sunlight and biomass to produce hydrogen under ambient conditions, holding a significant promise for future energy sustainability. However, the main challenge lies in developing highly active and stable photocatalysts with high light harvesting efficiency. In this study, we adopted a simple yet effective approach that combines thermal exfoliation and photodeposition to anchor Pt single atoms onto ultra-thin g-C_3N_4 nanosheets (MCNN). The incorporation of Pt single atoms induced a distinct red-shift in the visible light region, augmenting the solar energy absorption capacity, while the enlarged surface area of g-C_3N_4 nanosheets improved the mass transfer. Moreover, the enhanced photoelectric properties further contributed to the superior performance of Pt-MCNN-3.0 % in the photoreforming of glucose for hydrogen evolution. Remarkably, Pt-MCNN-3.0 % demonstrated an impressive hydrogen generation rate, approximately 59 times higher than that of MCNN, after a 3 h visible-light irradiation, maintaining a satisfied photo-stability. This work addresses the critical need for design of efficient photocatalysts, bringing us one step closer to realizing the potential of biomass photoreforming as a sustainable and clean energy conversion technology.

1. Introduction

Hydrogen, a renewable, clean, and sustainable energy source, is in high demand in the chemical industry and pharmaceutical synthesis [1, 2]. However, conventional H_2 generation technologies, for instance, steam reforming of methane, are hindered by their high energy consumption from critical reaction conditions. They require high temperature and pressure, resulting in the challenges related to catalyst stability and deactivation [3]. In contrast, photocatalytic water splitting reaction offers a greener approach to obtain hydrogen energy *via* a direct storage and conversion process of solar energy [4]. However, the use of sacrificial agents to trap hot holes in the intriguing process is often non-selective for CO_2, leading to increased energy consumption [5].

Biomass reforming is a process that converts plant-derived biomass energy resources into valuable products such as biofuels, hydrogen, or synthesis gas. Moreover, the integration of solar light harvesting and biomass reforming into a single process, known as photoreforming of biomass, has gained significant attention [6–9]. Compared to photocatalytic water splitting, biomass photoreforming offers higher hydrogen productivity because of the lower Gibbs free energy involvement and the production of highly valued fuels as the oxidation half-reaction product (Scheme 1a) [10]. As such, researchers have explored various photocatalysts and reactions for hydrogen generation *via* photoreforming since Kawai and Sakata's ground-breaking work in 1980 [11,12]. In this process, biomass serves as an electron donor that is to be oxidized by photoinduced holes for highly valued products, while the photoinduced electrons migrate to the photocatalyst surface to reduce water molecules, generating H_2 [13].

Among various biomass substrates, glucose, a type of polyol, exhibits a particularly high hydrogen evolution rate during photoreforming process owing to its simplified structure, making it an intriguing platform for understanding the photoreforming mechanism [14]. Moreover, the OH functional groups in glucose can be easily oxidized by holes to form hydroxyl radicals, acting as reactive oxidants in the photoreforming process [15]. In the realm of photocatalysis, two-dimensional semiconductors have garnered considerable attention because of their

* Corresponding author.
E-mail address: jinqiang.zhang@adelaide.edu.au (J. Zhang).

https://doi.org/10.1016/j.surfin.2023.103423
Received 1 August 2023; Received in revised form 10 September 2023; Accepted 19 September 2023
Available online 20 September 2023

excellent electronic conductivity and unique physiochemical properties [16]. Graphitic carbon nitride (g-C_3N_4) stands out as a non-toxic, metal-free, and visible-light-responsive photocatalytic nanomaterial, making it an excellent candidate for various photocatalytic applications [17–19]. However, 2D g-C_3N_4 faces challenges such as sluggish charge dynamics and a high probability of photoexcited electron-hole recombination, limiting its performance in photocatalysis (Scheme 1b) [20–22]. To address these issues, noble metals nanoparticles like Ag, Au, and Pt have been loaded onto the surface of g-C_3N_4 as co-catalysts to create Schottky heterojunctions, leveraging the surface plasmon resonance (SPR) effect to enhance the absorption of solar energy and improve charge separation and transportation [23–26]. Nevertheless, the practical application of Schottky heterojunctions in the photocatalytic reforming of biomass is hindered by the weak interfacial internal electric field and a low metal utilization efficiency.

In this study, we synthesized ultra-thin g-C_3N_4 nanosheets (MCNN) *via* thermal treatment of g-C_3N_4, followed by the photodeposition of varying amounts of Pt single atoms (isolated metal centres). We conducted an in-depth analysis of the physicochemical and optoelectrical properties of the prepared samples, emphasizing the advantages of single-atom catalysts. Furthermore, we monitored and evaluated the hydrogen evolution performance of these prepared samples during the photoreforming process of glucose. Additionally, we unveiled the reaction mechanism and structure-performance relationship of the single-atom-based photoreforming process of glucose. This innovative photocatalyst is expected to maximize the conversion of solar energy and biomass into hydrogen through photoreforming reactions.

2. Experimental section

2.1. Preparation of pristine g-C_3N_4

Pristine g-C_3N_4 was synthesized using a facile thermal polymerization process [27]. Specifically, 10 g of melamine was placed in a 50 mL crucible and heated up to 550 °C with a ramping rate of 5 °C min^{-1}. The mixture was then maintained in a muffle furnace for 2 h. After cooling down to 25 °C, the resulting yellowish products were ground into powders and labelled as MCN.

2.2. Preparation of ultra-thin g-C_3N_4

Ultra-thin g-C_3N_4 was synthesized using a thermal etching approach. MCN was placed in a porcelain boat without a cover and heated up to 500 °C under an air atmosphere at a ramping rate of 10 °C min^{-1}. After 2 h of heating, the yellowish powders were collected and denoted as MCNN.

2.3. Embed of Pt single atom on the host of MCNN

2, 4, 6, and 8 mL of chloroplatinic acid hydrate solution (1500 ppm) were diluted with 23, 21, 19 and 17 mL of ultra-pure water, respectively. Then, 0.2 g of MCNN was dispersed in each Pt solution using sonication for 30 min. The mixture was illuminated under a 300 W Xenon lamp with vigorous stirring for 1 h. The obtained substance was rinsed and centrifuged multiple times using anhydrous ethanol and ultra-pure water. The final material was dried overnight at 50 °C in a vacuum oven. The obtained photocatalysts were labelled as Pt/MCNN-1.5 %, Pt/MCNN-3.0 %, Pt/MCNN-4.5 %, and Pt/MCNN-6.0 %, respectively.

2.4. Characterizations

Various characterization techniques were employed to study the prepared samples. X-ray diffraction (XRD) patterns were obtained using a Panalytical Empyrean multipurpose research diffractometer with Cu Kα radiation. Fourier transform infrared (FT-IR) spectra were collected using a PerkinElmer UATR Two. High-resolution transmission electron microscopy (HRTEM) and transmission electron microscopy (TEM) images were captured using a FEI Titan G2 80-200 US TEM microscope. X-

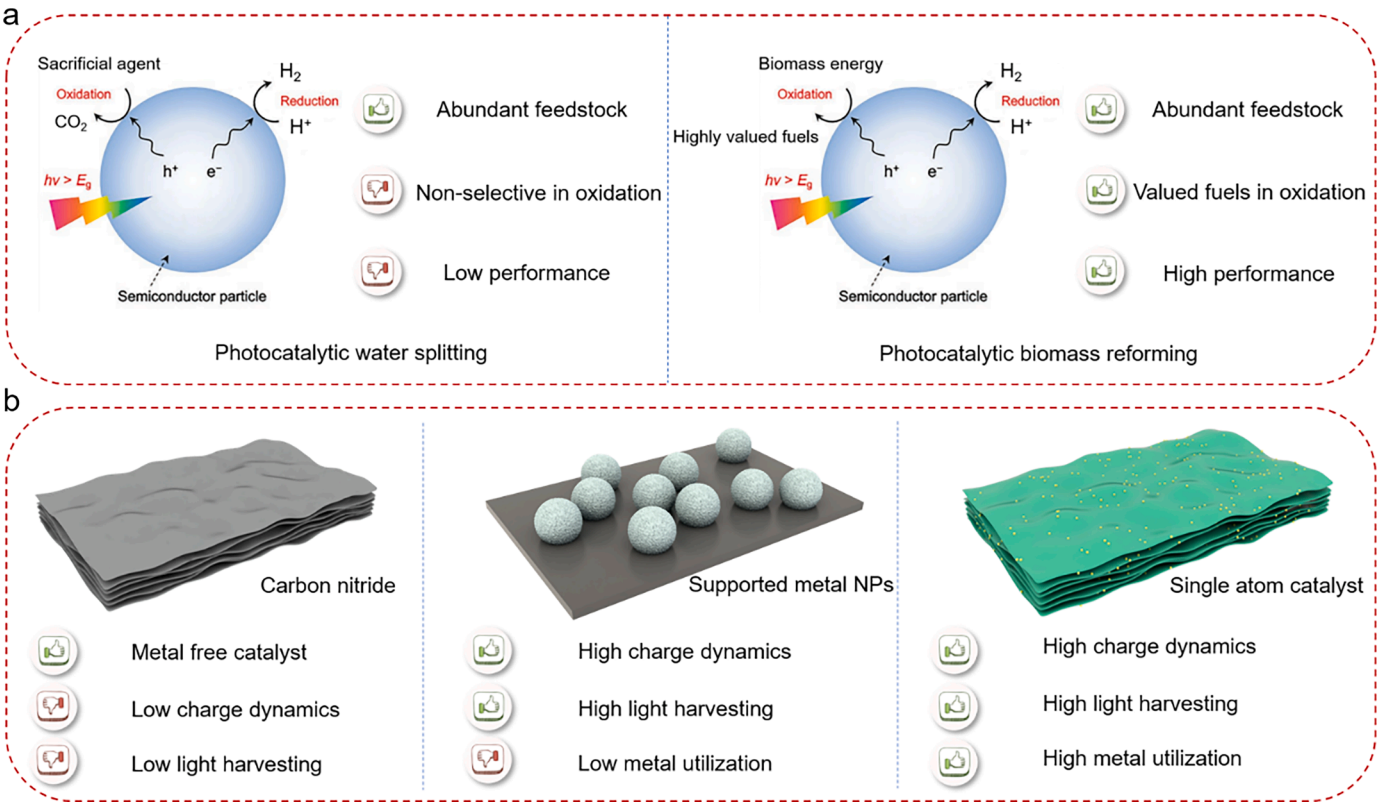

Scheme 1. Principles for (a) reaction engineer and (b) catalyst design.

ray photoelectron spectroscopy (XPS) spectra were acquired using an Escalabl 250XI (Al Kα X-ray) from Thermo Fisher Scientific. UV–Vis diffuse reflectance spectra (DRS) were recorded using an Agilent Cary 300 UV–Vis spectrophotometer with an integrated sphere. Brunauer–Emmett–Teller (BET) surface area and porous structure of the photocatalysts were measured using a micromeritics TriStar II (surface area and porosity). Transient-state photoluminescence (PL) spectra were collected on a FLS1000 spectrometer (Edinburgh Instruments, UK).

2.5. Photocatalytic activity evaluation

Photoreforming of biomass processes were conducted using a customized sealed quartz vessel with a top window. A 300 W Xeon lamp was used as the solar light source (150 mW/cm^{-2}) to initiate the photoreforming reaction. In a typical run, 25 mg of the prepared nanomaterial was mixed with 25 mL of glucose solution (96 ppm). Ultra-pure N_2 was used to purge the mixture for 30 min to remove the dissolved O_2. The generated hydrogen was monitored using an online gas chromatography (Shimadzu GC-2030 online, He carrier gas) with the PID detector.

3. Results and discussion

3.1. Catalyst preparation and characterization

The synthesis of Pt-MCNN samples employs a photodeposition process. To be more precise, this process involves the excitation of energetic hot carriers within the carbon nitride host when exposed to light. In this photoexcitation, hot electrons actively engage in the reduction of Pt ions. Consequently, the configuration of Pt on the carbon nitride substrate is strongly influenced by factors such as the Pt salt concentration, the intensity and duration of light irradiation, the specific nature of the host material, and the exposure time to light.

The morphology and microstructure of Pt-MCNN samples were extensively investigated using high-angle annular dark-field scanning transmission electron microscopy (HAADF-STEM) images (Fig. 1). The transition from graphitic carbon nitride (MCN) with a dense block nanostructure to MCNN, which displays ultra-thin nanosheets with nanopores throughout the in-plane, was observed after the thermal exfoliation process. Moreover, the images (Fig. 1a–c) illustrate the distinct features of Pt-MCNN-3.0 %, showcasing the laminar structure of carbon nitride nanosheets with a uniform distribution of Pt single atoms

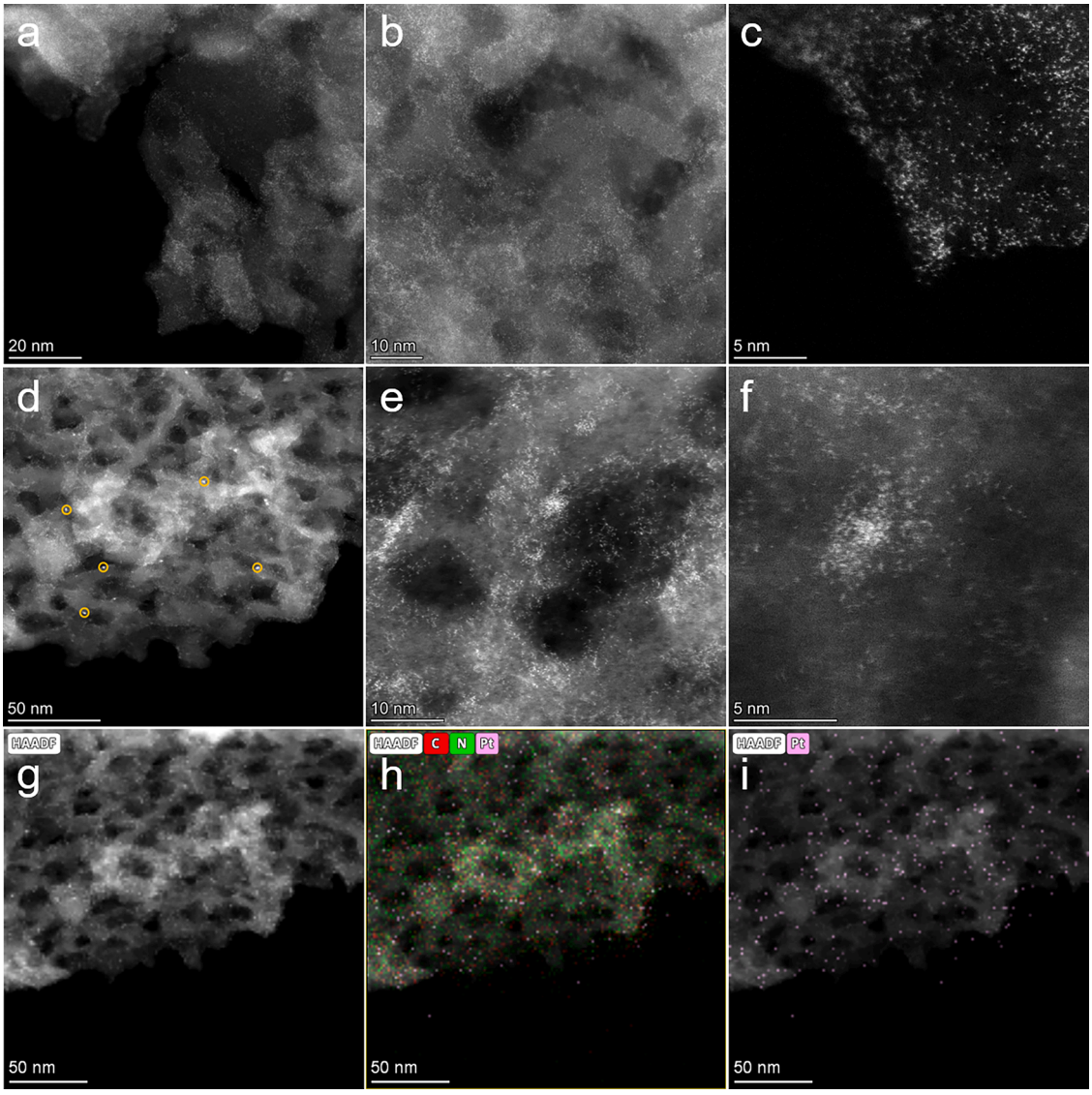

Fig. 1. HAADF-STEM images of Pt single atoms anchored on the host of MCNN. (a–c) HAADF-STEM images of Pt-MCNN-3.0 %, (d-f) HAADF-STEM images of Pt-MCNN-6.0 %, and (g–i) STEM-EDX element mapping images of Pt-MCNN-3.0 %.

(white dots) on the MCNN surface. Furthermore, increasing the Pt content during the preparation of Pt-MCNN resulted in shorter distances between Pt single atoms, leading to the formation of some nano clusters on Pt-MCNN-6.0 % (Fig. 1d–f). Despite the high loading of Pt, the framework of the carbon nitride host remained intact, demonstrating the stability of the material. EDX elemental mapping images of Pt-MCNN-3.0 % provided further evidence of the tight and uniform decoration of Pt single atoms on the surface of the ultra-thin and porous carbon nitride nanosheets (MCNN) (Figs. 1g–i and S1–3).

To investigate the crystalline structures of the prepared photocatalysts, XRD patterns were collected (Fig. 2a). A characteristic diffraction peak at 13.1° was observed, corresponding to the (100) facet of pristine MCNN, indicating the presence of in-plane periodic tri-s-triazine units [28]. Additionally, another diffraction peak at 27.7° was identified, corresponding to the (002) plane, representing the stacking of conjugated aromatic layers [29,30]. Notably, the diffraction peaks of Pt nanoparticles (with Pt-Pt bonding) were absent in all the Pt-MCNN samples, indicating that Pt metal was loaded on the MCNN in the form of isolated metal centres (without Pt-Pt bonding) [31].

FT-IR spectra of the prepared samples were recorded in the range of 500 to 3500 cm^{-1}, as shown in Fig. 2b. A broad peak observed from 3100 to 3500 cm^{-1} was ascribed to the stretching of N-H and O-H. Furthermore, characteristic peaks at 1228, 1328, 1428, 1557, and 1632 cm^{-1} were identified, corresponding to the stretching vibration mode of C-N heterocyclic compounds [32]. Another distinctive peak at 806 cm^{-1} was attributed to the tri-s-triazine units. Importantly, all the Pt single atom modified MCNN materials exhibited similar stretching peaks compared to MCNN, indicating that loading Pt nanoparticles on MCNN did not disrupt the molecular structure of the MCNN substrate. These results are consistent with the maintained morphology observed in the HAADF-STEM images.

N_2 adsorption-desorption isotherms were employed to study the textural properties of the synthesized samples (Fig. 2c). The results revealed a slight increase in the specific Brunauer–Emmett–Teller (BET) surface area after loading Pt nanoparticles on MCNN, with values of 153.1 and 144.7 m^2/g for Pt/MCNN-3.0 % and MCNN, respectively (Table S1). Additionally, the pore size distribution results indicated that the modification of MCNN with Pt nanoparticles did not affect the pore structure of MCNN (Fig. 2d). This finding is consistent with the conclusions drawn from FTIR and HAADF-STEM results, indicating that loading Pt single atoms on MCNN cannot change the framework of carbon nitride substrate.

The surface chemical states of MCNN and Pt/MCNN-3.0 % were analyzed using X-ray photoelectron spectroscopy (XPS). As shown in Fig. 3a, the XPS survey spectrum displayed the presence of three elements (C, N, and O) on both samples, with a small amount of Pt detected on Pt/MCNN-3.0 %. The C and N signals originated from the carbon nitride substrate, while the O signal was attributed to the partial oxidation of MCNN and adsorbed water on the catalyst surface. C 1s spectra (Fig. 3b) showed two peaks at 284.6 and 287.9 eV for both samples, corresponding to sp^2 C-C bonds and sp^2-bonded carbon (N-C=N) of the s-triazine rings [27,33,34]. Interestingly, the bonding energy of these two peaks remained unchanged after Pt loading on MCNN, indicating no significant interaction between Pt and C atoms in Pt-MCNN-3.0 %. Furthermore, the N 1s XPS spectra of MCNN (Fig. 3c) were deconvolved into three peaks at 400.5, 398.6, and 398.3 eV, corresponding to sp^2-bonded nitrogen C-N=C, tertiary N atoms in H-N-$(C)_3$, and C-NH_x, respectively [28,35–37]. However, in Pt-MCNN-3.0 %, the

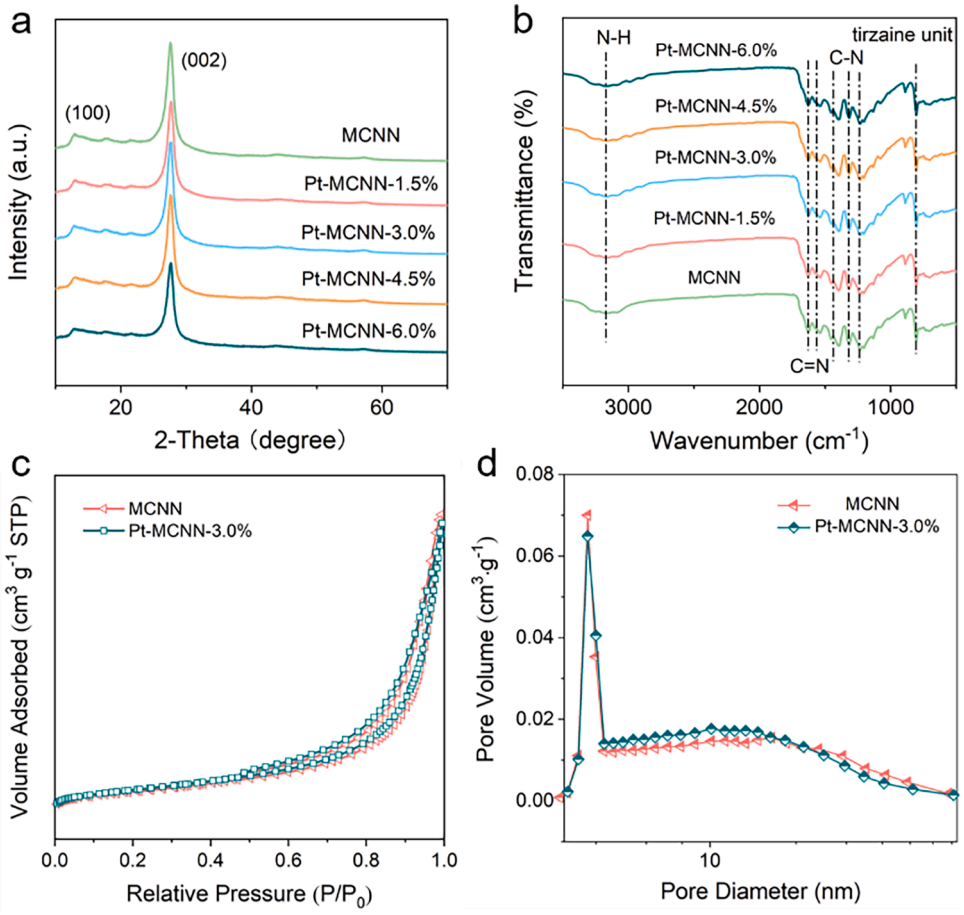

Fig. 2. Catalyst characterizations. (a) XRD patterns, (b) FT-IR spectra, (c) nitrogen adsorption-desorption isotherms, and (d) distributions of pore size of pristine MCNN and Pt-MCNN-3.0 %.

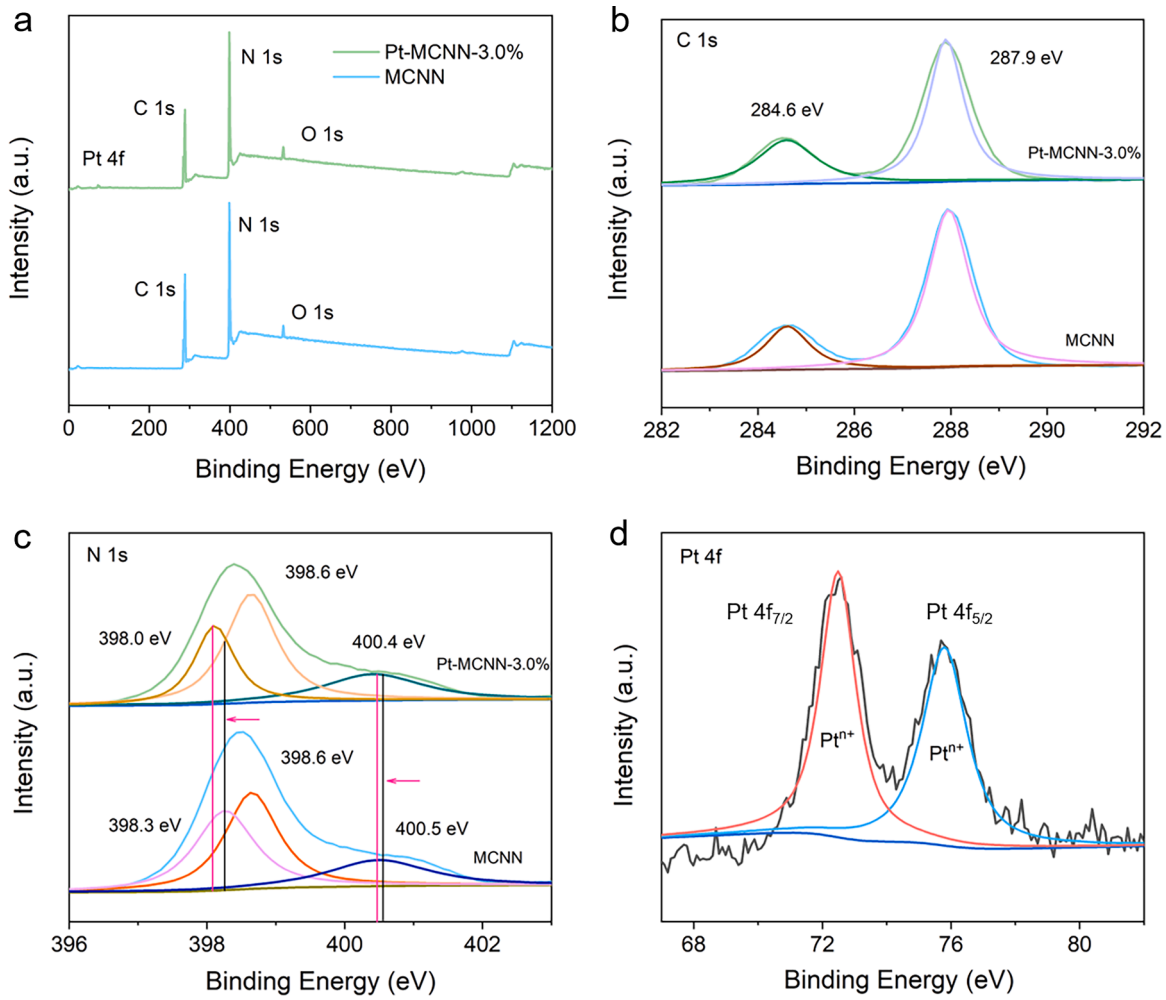

Fig. 3. XPS spectra of Pt-MCNN-3.0 % and pure MCNN. (a) XPS survey spectrum, XPS spectra of (b) C 1s, (c) N 1s and (d) Pt 4f.

peaks of sp^2-bonded nitrogen C-N=C and C-NH_x decreased to 400.4 and 398.0 eV, respectively, suggesting electron transfer between Pt and N atoms in Pt-MCNN-3.0 %. Additionally, the presence of Pt $4f^{7/2}$ and Pt $4f^{5/2}$ peaks at 72.6 and 76.0 eV (Fig. 3d) indicated the existence of Pt^{n+} species. Consequently, Pt was incorporated into the MCNN host in the form of Pt-N coordination, leading to a charge pumping effect on photo-excited charge carriers and boosting charge dynamics in Pt-MCNN-3.0 %.

UV-Vis spectra of all the synthesized photocatalysts were obtained to assess their photo absorption capabilities, as shown in Fig. 4a. MCNN displayed a marginal absorption edge at around 480 nm, indicating its responsiveness to visible light. Upon Pt single atom modification in Pt-MCNN samples, slight red-shift and Urbach tails were observed, signifying an improvement in light harvesting efficiency. It should be noted that compared to Pt-MCNN-4.5 %, a blue-shift appeared on Pt-MCNN-6.0 %, indicating the light absorption ability of nano cluster was lower than that of isolated metal centers. The bandgap energies of MCNN and Pt-MCNN-3.0 % were determined using Tauc's equation: $(\alpha hv)^n = k(hv - E_g)$, where n = 1/2 (for a direct semiconductor), and the corresponding plots are presented in Fig. 4b and c [38,39]. The band gap was narrowed by 0.04 eV after embedding of Pt single atoms on MCNN. Furthermore, the XPS valence band spectra of MCNN and Pt-MCNN-3.0 % were acquired to elucidate their band structures (Fig. 4d and e). Compared to MCNN, the conduction band of Pt-MCNN-3.0 % was heightened, suggesting an enhanced hydrogen reduction ability (Figs. 4f and S4).

The optical-electrical properties of the prepared samples were studied. The separation capability of photo-excited charge carriers in the prepared samples was initially studied using fluorescence (PL) spectra (Fig. 5a). A noticeable peak can be observed on all the samples, of which a higher peak intensity typically represented a faster recombination rate of charge carriers. Compared to MCNN, the peak intensity of Pt-MCNN-3 % was significantly reduced, indicating the pumping effect of isolated Pt centres on promoting the separation of excitons. The peak was intensified further increasing the Pt loading in Pt-MCNN-6 %, manifesting that nano-cluster was more beneficial for trapping hot carriers for recombination. Similarly, electrochemical impedance spectroscopy (EIS) was conducted to study the interfacial resistance for the charge transport of all the synthesized samples (Fig. 5b). The arc radius of Pt-MCNN-3 % turned smaller after the fabrication of single atom catalyst, exhibiting the high mobility of charge transportation in Pt-MCNN-3 %. Combined with the faster separation and transportation of charge carriers, Pt-MCNN-3 % exhibited the highest photocurrent among all the samples (Fig. 5c).

3.2. Photocatalytic hydrogen production

The performance of photoreforming over the prepared nanomaterials was performed through batch scale tests using a D-+-glucose aqueous solution as a simplified model compound of biomass. The photocatalytic reforming process was carried out by irradiating the solution for 3 h at 30 °C.

Initial experiments were carried out without either light irradiation or catalysts, yet we were unable to detect any hydrogen production. This

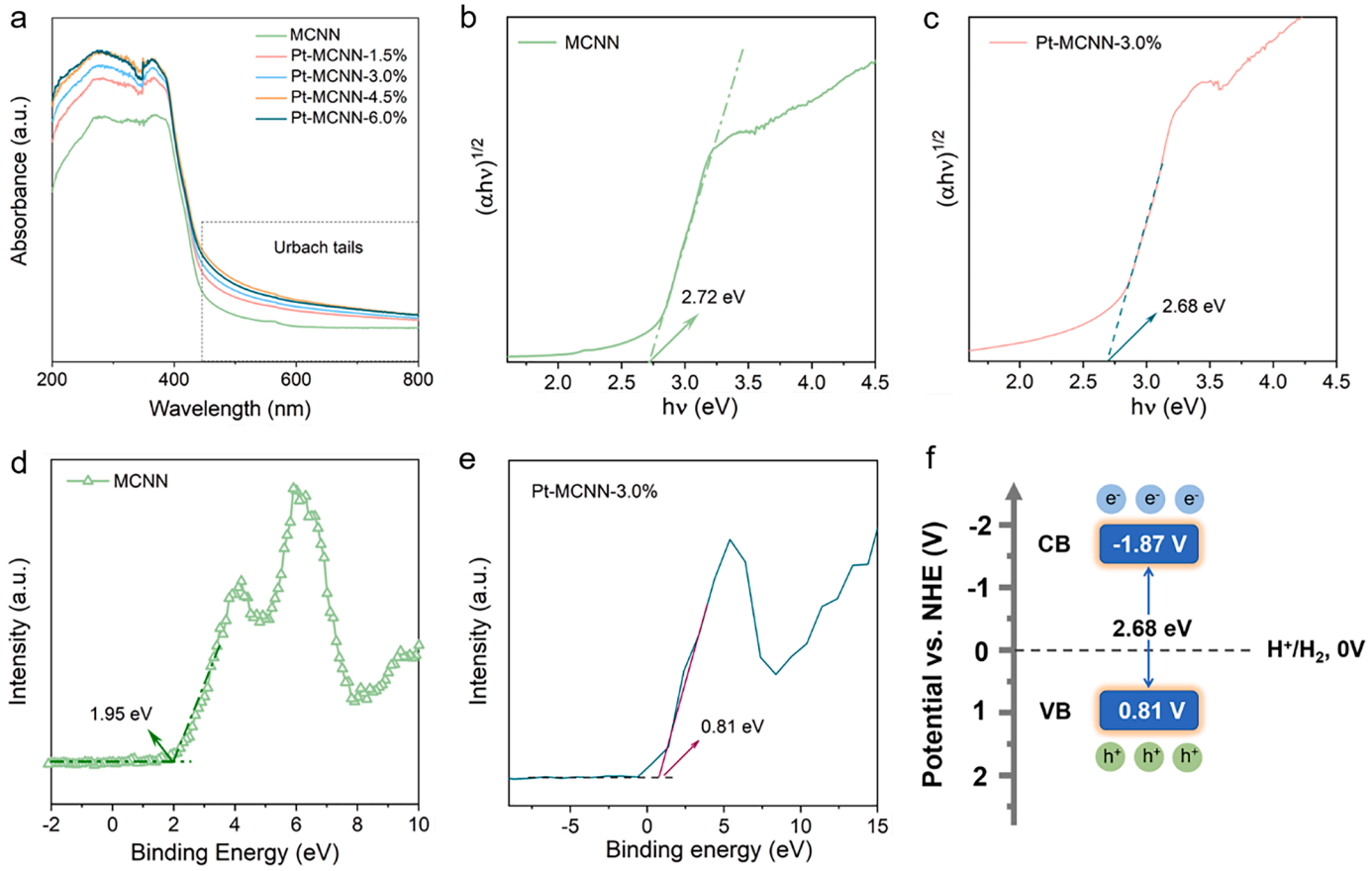

Fig. 4. Study of band structures of the prepared samples. (a) UV-Vis DRS spectra of all the prepared catalysts, Tauc's plots of (b) MCNN and (c) Pt-MCNN-3.0 %, XPS valence band spectrum of (d) MCNN and (e) Pt-MCNN-3.0 %, and (f) band structure of Pt-MCNN-3.0 %.

underscores the crucial role played by both light and catalysts in the process of photocatalysis. As shown in Fig. 5d, the lowest hydrogen production rate (3.41 μmol g^{-1}) was observed for pristine MCNN. In contrast, a significant improvement in hydrogen evolution was evident after incorporating Pt single atoms into the carbon nitride host. Notably, Pt-MCNN-3.0 % exhibited an impressive hydrogen production rate of 201.23 μmol g^{-1} in a 3 h reaction, which is 59 times higher than that of MCNN. However, we did not observe further enhancement in hydrogen reduction with Pt-MCNN-6.0 % compared to Pt-MCNN-3.0 %, as the single atoms agglomerated into clusters. Although synergy effect has widely been reported between Pt nanoparticles and Pt single atoms, the photocatalytic performance of Pt-MCNN-6.0 % remained lower than Pt-MCNN-3.0 % [40–42]. Additionally, we loaded Pt nanoparticles (NPs) onto MCNN and MCN, which showed a low photocatalytic performance in the photoreforming of glucose (Fig. 5e), fully suggesting the higher catalytic performance of isolated Pt centres than Pt nanoparticles. The photo stability of Pt-MCNN-3.0 % during the photoreforming process of glucose was measured and maintained at a high-performance level, indicating a satisfactory stability of Pt single atoms for hydrogen production (Fig. 5f). Therefore, the impressive enhancement of Pt-MCNN-3.0 % in the photoreforming of glucose can be attributed to the formation of isolated Pt centres, which act as pumps, efficiently increasing the separation and mobility of hot carriers for redox reactions.

3.3. *Photocatalytic mechanism of the reforming reactions*

Based on the comprehensive analysis, a plausible reaction mechanism for the photoreforming of glucose using Pt-MCNN-3.0 % is proposed and depicted in Fig. 6. Upon absorption of solar energy, photo-generated electrons in MCNN move from the valence band (VB) to the conduction band (CB), while holes with a strong oxidation capability remain in the VB. The incorporation of Pt single atoms in the form of Pt-N coordination enhances visible light absorption and, importantly, acts as 'pumps' that facilitate the efficient separation of electron-hole pairs, leading to the accumulation of more energetic hot electrons at the isolated Pt centres [23,24,43]. These highly energetic hot electrons at the CB of Pt-MCNN-3.0 % play a significant role in driving the reduction reaction, converting H^+ to liberate green hydrogen. Besides, the enlarged surface area of Pt-MCNN-3.0 % accelerated the mass transferring for an enhanced reaction kinetics. Simultaneously, the photoinduced holes trigger the oxidation of glucose, resulting in the production of various products, such as arabinose, erythrose, and formic acid [44,45]. Consequently, the photoreforming process efficiently utilizes solar energy to convert glucose into valuable products and generate green hydrogen energy.

4. Conclusion

In conclusion, the photoreforming performance of MCNN nanosheets, derived from melamine, can be significantly enhanced by decorating Pt single atoms in its matrix, benefiting from the pumping effect of isolated Pt centres on photo-excited charge carriers. The formed Pt-N coordination plays a crucial role in efficiently promoting charge carriers' separation, thereby reducing their recombination after the decoration Pt single atom on the host of MCNN. Moreover, the incorporation of Pt particles on MCNN results in a red shift in the absorption spectrum, indicating a higher light absorption capacity as compared to pure MCNN. Furthermore, the enlarged surface area after Pt single atom decoration promoted mass transferring. As such, the highest

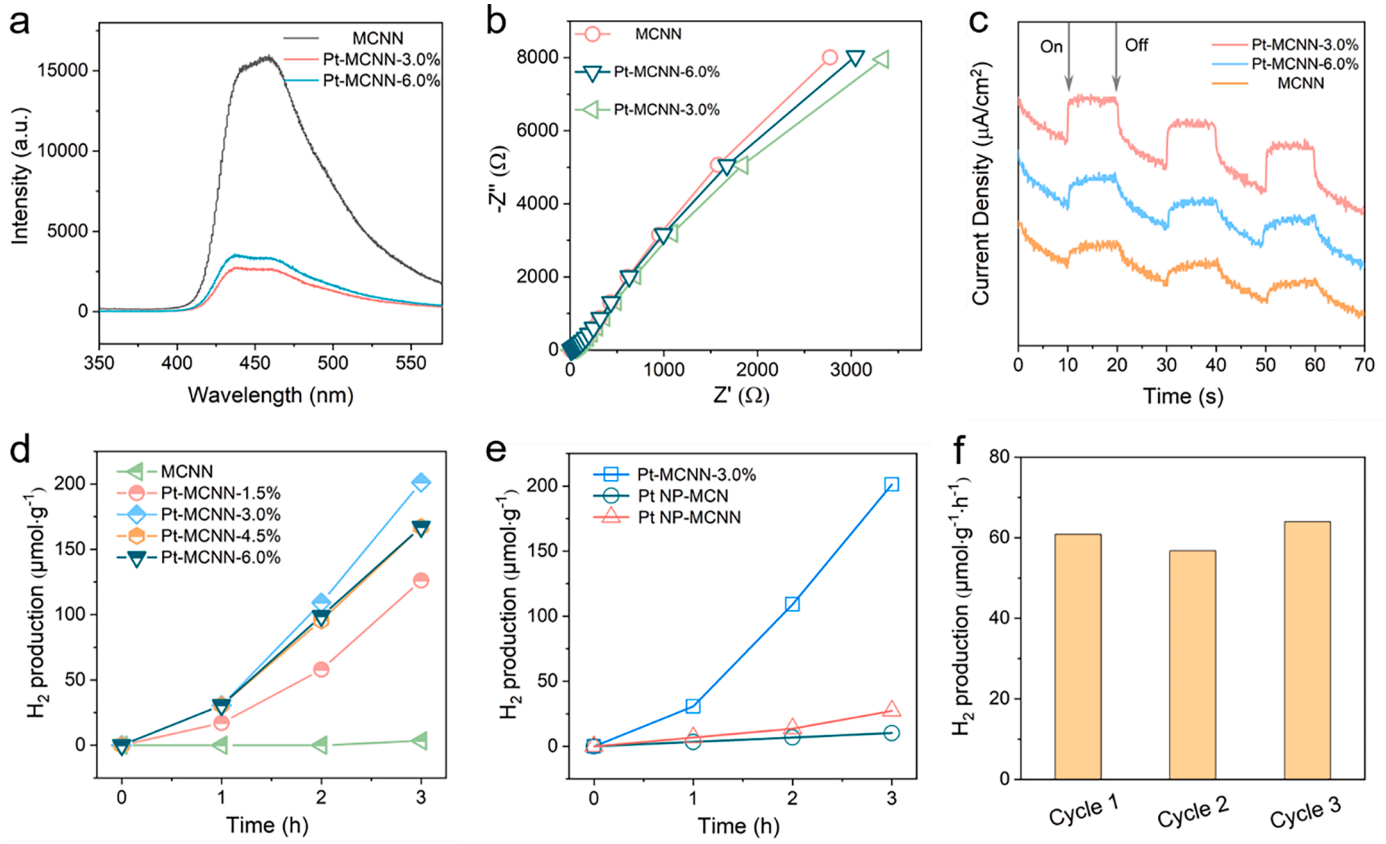

Fig. 5. (a) PL spectra, (b) EIS curves and (c) photocurrent of MCNN, Pt-MCNN-3.0 % and Pt-MCNN-6.0 %, (d) hydrogen evolution of MCNN and Pt single atom loaded MCNN in photoreforming of glucose aqueous solution, (e) hydrogen production on Pt-MCNN-3.0 % and Pt nanoparticles loaded on MCN and MCNN in photoreforming of glucose aqueous solution, and (f) stability test of Pt-MCNN-3.0 % in photoreforming of glucose aqueous solution.

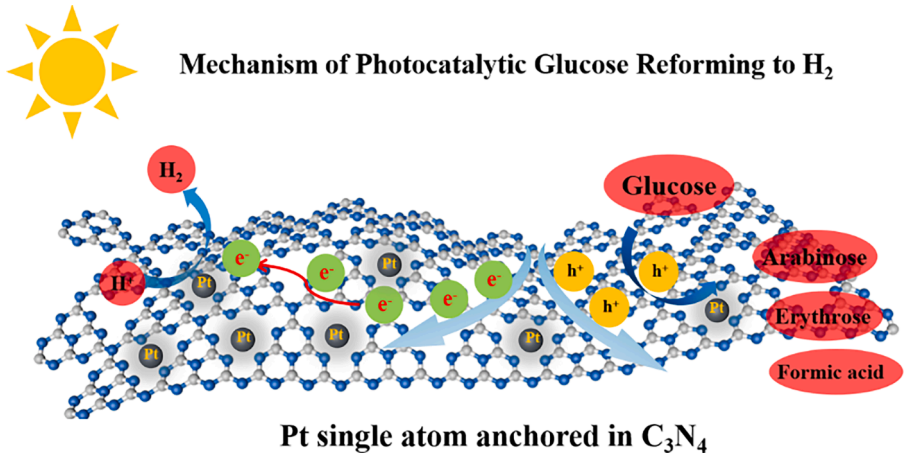

Fig. 6. The proposed mechanism of photoreforming of glucose over Pt-MCNN-3.0 %.

performance (201.23 μmol g^{-1}), which is 59 times higher than pristine MCNN, is achieved on Pt-MCNN-3.0 %, which remarkably outperformed MCNN and MCN supported Pt nanoparticles catalysts. This study offers advanced photocatalysts in utilizing solar energy and biomass for green hydrogen generation.

CRediT authorship contribution statement

Jinqiang Zhang: Methodology, Data curation, Writing – original draft, Visualization. **Xinyuan Xu:** Investigation, Validation. **Yazi Liu:** Software. **Xiaoguang Duan:** Validation, Data curation. **Shaobin Wang:** Supervision, Project administration. **Hongqi Sun:** Supervision, Conceptualization, Writing – review & editing.

Declaration of Competing Interest

The authors declare that they have no known competing financial interests or personal relationships that could have appeared to influence the work reported in this paper.

Data availability

Data will be made available on request.

Acknowledgment

This work was supported by the Australian Research Council (DP200103206).

Supplementary materials

Supplementary material associated with this article can be found, in the online version, at doi:10.1016/j.surfin.2023.103423.

References

[1] H. Nishiyama, T. Yamada, M. Nakabayashi, Y. Maehara, M. Yamaguchi, Y. Kuromiya, Y. Nagatsuma, H. Tokudome, S. Akiyama, T. Watanabe, R. Narushima, S. Okunaka, N. Shibata, T. Takata, T. Hisatomi, K. Domen, Photocatalytic solar hydrogen production from water on a 100-m(2) scale, Nature 598 (2021) 304–307.
[2] P. Zhou, I.A. Navid, Y. Ma, Y. Xiao, P. Wang, Z. Ye, B. Zhou, K. Sun, Z. Mi, Solar-to-hydrogen efficiency of more than 9% in photocatalytic water splitting, Nature 613 (2023) 66–70.
[3] H. Zhang, Z. Sun, Y.H. Hu, Steam reforming of methane: current states of catalyst design and process upgrading, Renew. Sustain. Energy Rev. 149 (2021), 111330.
[4] D. Zhao, Y. Wang, C.-L. Dong, Y.-C. Huang, J. Chen, F. Xue, S. Shen, L. Guo, Boron-doped nitrogen-deficient carbon nitride-based Z-scheme heterostructures for photocatalytic overall water splitting, Nat. Energy 6 (2021) 388–397.
[5] J. Zhang, X. Tan, L. Shi, H. Chen, Y. Liu, S. Wang, X. Duan, M. Wu, H. Sun, S. Wang, Tandem internal electric fields in intralayer/interlayer carbon nitride homojunction with a directed flow of photo-excited electrons for photocatalysis, Appl. Catal. B Environ. 333 (2023), 122781.
[6] S.J.A. Moniz, S.A. Shevlin, D.J. Martin, Z.-X. Guo, J. Tang, Visible-light driven heterojunction photocatalysts for water splitting – a critical review, Energy Environ. Sci. 8 (2015) 731–759.
[7] X. Liu, X. Wu, J. Li, L. Liu, Y. Ma, Simple synthesis of oxygen functional layered carbon nitride with near-infrared light photocatalytic activity, Catal. Commun. 91 (2017) 21–24.
[8] K.C. Christoforidis, Z. Syrgiannis, V.L. Parola, T. Montini, C. Petit, E. Stathatos, R. Godin, J.R. Durrant, M. Prato, P. Fornasiero, Metal-free dual-phase full organic carbon nanotubes/g-C_3N_4 heteroarchitectures for photocatalytic hydrogen production, Nano Energy 50 (2018) 468–478.
[9] X. Xu, L. Shi, S. Zhang, Z. Ao, J. Zhang, S. Wang, H. Sun, Photocatalytic reforming of lignocellulose: a review, Chem. Eng. J. 469 (2023), 143972.
[10] K.C. Christoforidis, P. Fornasiero, Photocatalytic hydrogen production: a rift into the future energy supply, ChemCatChem 9 (2017) 1523–1544.
[11] T. Kawai, T. Sakata, Conversion of carbohydrate into hydrogen fuel by a photocatalytic process, Nature 286 (1980) 474–476.
[12] A.V. Puga, Photocatalytic production of hydrogen from biomass-derived feedstocks, Coord. Chem. Rev. 315 (2016) 1–66.
[13] M.F. Kuehnel, E. Reisner, Solar hydrogen generation from lignocellulose, Angew. Chem. Int. Ed. 57 (2018) 3290–3296.
[14] A. Speltini, A. Scalabrini, F. Maraschi, M. Sturini, A. Pisanu, L. Malavasi, A. Profumo, Improved photocatalytic H_2 production assisted by aqueous glucose biomass by oxidized g-C_3N_4, Int. J. Hydrogen Energy 43 (2018) 14925–14933.
[15] I. Rossetti, Hydrogen production by photoreforming of renewable substrates, Int. Sch. Res. Notices 2012 (2012), 964936.
[16] X. Xu, J. Zhang, S. Wang, Z. Yao, H. Wu, L. Shi, Y. Yin, S. Wang, H. Sun, Photocatalytic reforming of biomass for hydrogen production over ZnS nanoparticles modified carbon nitride nanosheets, J. Colloid Interface Sci. 555 (2019) 22–30.
[17] A. Deng, Y. Sun, Z. Gao, S. Yang, Y. Liu, H. He, J. Zhang, S. Liu, H. Sun, S. Wang, Internal electric field in carbon nitride-based heterojunctions for photocatalysis, Nano Energy 108 (2023), 108228.
[18] J. Qin, J. Barrio, G. Peng, J. Tzadikov, L. Abisdris, M. Volokh, M. Shalom, Direct growth of uniform carbon nitride layers with extended optical absorption towards efficient water-splitting photoanodes, Nat. Commun. 11 (2020) 4701.
[19] J. Zhang, Y. Li, X. Zhao, L. Wang, H. Chen, S. Wang, X. Xu, L. Shi, L.-C. Zhang, Y. Zhu, H. Zhang, Y. Liu, G. Nealon, S. Zhang, M. Wu, S. Wang, H. Sun, Aligning potential differences within carbon nitride based photocatalysis for efficient solar energy harvesting, Nano Energy 89 (2021), 106357.
[20] W. Wu, J. Zhang, W. Fan, Z. Li, L. Wang, X. Li, Y. Wang, R. Wang, J. Zheng, M. Wu, H. Zeng, Remedying defects in carbon nitride to improve both photooxidation and H_2 generation efficiencies, ACS Catal. 6 (2016) 3365–3371.
[21] D. Hao, Q. Huang, W. Wei, X. Bai, B.-J. Ni, A reusable, separation-free and biodegradable calcium alginate/g-C_3N_4 microsphere for sustainable photocatalytic wastewater treatment, J. Clean. Prod. 314 (2021), 128033.
[22] C.-C. Wang, X.-H. Yi, P. Wang, Powerful combination of MOFs and C_3N_4 for enhanced photocatalytic performance, Appl. Catal. B Environ. 247 (2019) 24–48.
[23] Z. Liu, W. Hou, P. Pavaskar, M. Aykol, S.B. Cronin, Plasmon resonant enhancement of photocatalytic water splitting under visible illumination, Nano Lett. 11 (2011) 1111–1116.
[24] Y. Yang, Y. Guo, F. Liu, X. Yuan, Y. Guo, S. Zhang, W. Guo, M. Huo, Preparation and enhanced visible-light photocatalytic activity of silver deposited graphitic carbon nitride plasmonic photocatalyst, Appl. Catal. B Environ. 142-143 (2013) 828–837.
[25] D. Hao, Y. Liu, S. Gao, H. Arandiyan, X. Bai, Q. Kong, W. Wei, P.K. Shen, B.-J. Ni, Emerging artificial nitrogen cycle processes through novel electrochemical and photochemical synthesis, Mater. Today 46 (2021) 212–233.
[26] X.-H. Yi, S.-Q. Ma, X.-D. Du, C. Zhao, H. Fu, P. Wang, C.-C. Wang, The facile fabrication of 2D/3D Z-scheme g-C_3N_4/UiO-66 heterojunction with enhanced photocatalytic Cr(VI) reduction performance under white light, Chem. Eng. J. 375 (2019), 121944.
[27] X. Wang, K. Maeda, A. Thomas, K. Takanabe, G. Xin, J.M. Carlsson, K. Domen, M. Antonietti, A metal-free polymeric photocatalyst for hydrogen production from water under visible light, Nat. Mater. 8 (2009) 76–80.
[28] S. Cao, J. Low, J. Yu, M. Jaroniec, Polymeric photocatalysts based on graphitic carbon nitride, Adv. Mater. 27 (2015) 2150–2176.
[29] J. Chen, Z. Hong, Y. Chen, B. Lin, B. Gao, One-step synthesis of sulfur-doped and nitrogen-deficient g-C_3N_4 photocatalyst for enhanced hydrogen evolution under visible light, Mater. Lett. 145 (2015) 129–132.
[30] H. Ou, L. Lin, Y. Zheng, P. Yang, Y. Fang, X. Wang, Tri-s-triazine-based crystalline carbon nitride nanosheets for an improved hydrogen evolution, Adv. Mater. 29 (2017), 1700008.
[31] Z. Wang, X. Peng, S. Tian, Z. Wang, Enhanced hydrogen production from water on Pt/g-C_3N_4 by room temperature electron reduction, Mater. Res. Bull. 104 (2018) 1–5.
[32] S. Tian, H. Ren, Z. Liu, Z. Miao, L. Tian, J. Li, Y. Liu, S. Wei, P. Wang, ZnS/g-C_3N_4 heterojunction with Zn-vacancy for efficient hydrogen evolution in water splitting driven by visible light, Catal. Commun. 164 (2022), 106422.
[33] L. Yang, X. Liu, Z. Liu, C. Wang, G. Liu, Q. Li, X. Feng, Enhanced photocatalytic activity of g-C_3N_4 2D nanosheets through thermal exfoliation using dicyandiamide as precursor, Ceram. Int. 44 (2018) 20613–20619.
[34] J. Li, G. Zhan, Y. Yu, L. Zhang, Superior visible light hydrogen evolution of Janus bilayer junctions *via* atomic-level charge flow steering, Nat. Commun. 7 (2016) 11480.
[35] L. Ge, C. Han, X. Xiao, L. Guo, Synthesis and characterization of composite visible light active photocatalysts MoS_2–g-C_3N_4 with enhanced hydrogen evolution activity, Int. J. Hydrogen Energy 38 (2013) 6960–6969.
[36] P. Chen, P. Xing, Z. Chen, H. Lin, Y. He, Rapid and energy-efficient preparation of boron doped g-C_3N_4 with excellent performance in photocatalytic H_2-evolution, Int. J. Hydrogen Energy 43 (2018) 19984–19989.
[37] W. Wang, Q. Niu, G. Zeng, C. Zhang, D. Huang, B. Shao, C. Zhou, Y. Yang, Y. Liu, H. Guo, W. Xiong, L. Lei, S. Liu, H. Yi, S. Chen, X. Tang, 1D porous tubular g-C_3N_4 capture black phosphorus quantum dots as 1D/0D metal-free photocatalysts for oxytetracycline hydrochloride degradation and hexavalent chromium reduction, Appl. Catal. B Environ. 273 (2020), 119051.
[38] Q. Han, B. Wang, J. Gao, Z. Cheng, Y. Zhao, Z. Zhang, L. Qu, Atomically thin mesoporous nanomesh of graphitic C_3N_4 for high-efficiency photocatalytic hydrogen evolution, ACS Nano 10 (2016) 2745–2751.
[39] Y. Liu, X. Xu, J. Zhang, H. Zhang, W. Tian, X. Li, M.O. Tade, H. Sun, S. Wang, Flower-like MoS_2 on graphitic carbon nitride for enhanced photocatalytic and electrochemical hydrogen evolutions, Appl. Catal. B Environ. 239 (2018) 334–344.
[40] Y. Yu, X. Dong, P. Chen, Q. Geng, H. Wang, J. Li, Y. Zhou, F. Dong, Synergistic effect of Cu single atoms and Au-Cu alloy nanoparticles on TiO(2) for efficient CO (2) photoreduction, ACS Nano 15 (2021) 14453–14464.
[41] X. Yang, Y. Wang, X. Wang, B. Mei, E. Luo, Y. Li, Q. Meng, Z. Jin, Z. Jiang, C. Liu, J. Ge, W. Xing, CO-tolerant PEMFC anodes enabled by synergistic catalysis between iridium single-atom sites and nanoparticles, Angew. Chem. Int. Ed. 60 (2021) 26177–26183.
[42] L. Kuai, Z. Chen, S. Liu, E. Kan, N. Yu, Y. Ren, C. Fang, X. Li, Y. Li, B. Geng, Titania supported synergistic palladium single atoms and nanoparticles for room temperature ketone and aldehydes hydrogenation, Nat. Commun. 11 (2020) 48.
[43] D.B. Ingram, P. Christopher, J.L. Bauer, S. Linic, Predictive model for the design of plasmonic metal/semiconductor composite photocatalysts, ACS Catal. 1 (2011) 1441–1447.
[44] R. Chong, J. Li, Y. Ma, B. Zhang, H. Han, C. Li, Selective conversion of aqueous glucose to value-added sugar aldose on TiO_2-based photocatalysts, J. Catal. 314 (2014) 101–108.
[45] M. Bellardita, E.I. García-López, G. Marcì, G. Nasillo, L. Palmisano, Photocatalytic solar light H_2 production by aqueous glucose reforming, Eur. J. Inorg. Chem. 2018 (2018) 4522–4532.